JOURNAL OF GEOPHYSICAL RESEARCH: ATMOSPHERES, VOL. 118, 8897–8909, doi:10.1002/jgrd.50705, 2013

A stochastic parameterization of the gravity waves due to convection and its impact on the equatorial stratosphere

F. Lott[1] and L. Guez[1]

Received 27 March 2013; revised 22 July 2013; accepted 2 August 2013; published 26 August 2013.

[1] A formalism is proposed to parameterize the gravity waves due to convection in general circulation models with a stratosphere. It is based on a stochastic approach, where a large ensemble of monochromatic gravity waves is built up by launching a few waves at each time step, and by adding the effect of these waves, to that of the waves launched before, during the same day. The frequency and horizontal wave numbers of each wave are chosen randomly with fixed probability distribution, but the wave amplitude is directly related to precipitation, which is converted into heating rate. Linear theory is then used to predict the gravity wave generated by the heating rate. Off-line tests are carried out using reanalysis and global precipitation data. These tests demonstrate that the scheme launches gravity wave momentum fluxes that are much more erratic in amplitude than when uniform sources are considered. Consequently, the scheme tends to produce momentum flux deposition at lower levels than for the case when uniform sources are considered. We verify that the parameterization, when included in a general circulation model with vertical resolution in the stratosphere $\delta z \approx 500$m, is able to produce a quasi-biennial oscillation, without being detrimental to other aspects of the model climatology, like the semiannual oscillation and the behavior of the extratropics.

Citation: Lott, F., and L. Guez (2013), A stochastic parameterization of the gravity waves due to convection and its impact on the equatorial stratosphere, *J. Geophys. Res. Atmos.*, *118*, 8897–8909, doi:10.1002/jgrd.50705.

1. Introduction

[2] The parameterization of gravity waves (GWs) is critical to the proper representation of the circulations of both the troposphere and the middle atmosphere in general circulation models (GCMs). In the midlatitude troposphere, the drag generated by orographic GWs helps to reduce temperature bias near the polar tropopause [*Palmer et al.*, 1986], contribute to the low-level mountain drag that corrects errors on the large scale flow near the surface [*Lott and Miller*, 1997], and affect the midlatitude stationary planetary waves [*Lott*, 1999]. In the middle atmosphere at midlatitudes, the momentum flux deposition due to nonstationary (i.e., nonorographic) GWs is acknowledged to be responsible for the reversal of the temperature gradient at the mesopause and to the formation of the summer cold mesopause [*Holton*, 1983]. Although in the middle atmosphere, the orographic GWs play a substantial role [*Lott et al.*, 2005; *McLandress and Shepherd*, 2009; *McLandress et al.*, 2013], it is nevertheless largely recognized that the significance of the nonorographic GWs is as important as that of the orographic ones [*Dunkerton*, 1982].

[3] In the equatorial regions, it is also well established that the nonorographic GWs are a substantial driver of the quasi-biennial oscillation QBO, *Lindzen and Holton* [1968], complementing the forcing from the synoptic and planetary scale equatorial waves that GCMs can resolve explicitly [see, for instance, *Lindzen and Tsay*, 1975; *Takahashi and Boville*, 1992; *Dunkerton*, 1997]. Today, it is well recognized that a broad spectrum of waves must be considered, and in most models with an internally generated QBO, the parameterized GWs contribute at least as much as the resolved waves [*Giorgetta et al.*, 2006].

[4] In order to parameterize the nonorographic GWs, some schemes like *Alexander and Dunkerton* [1999] or *Scinocca* [2003], bin the spectral domain by a large number of monochromatic waves, and treat the breaking of each of them quite independently from the others, for instance, by following *Lindzen* [1981]. Nevertheless, these "multiwaves" techniques are potentially expensive, since one needs a very good spectral resolution to adequately resolve critical levels [*Martin and Lott*, 2007]. Also, these schemes neglect the fact that during breaking, the different harmonics can interact, simply because breaking is a nonlinear process. In order to circumvent these two problems, some of the parameterizations developed in the 1990s have treated the GW spectra globally, largely using the observational fact that the spectra have well-known slopes along, for instance, their vertical wave number [*Hines*, 1997; *Warner and McIntyre*, 1996; *Manzini et al.*, 1997; *Scinocca*, 2003; *Orr et al.*, 2010].

[1]Laboratoire de Météorologie Dynamique, Ecole Normale Supérieure, Paris, France.

Corresponding author: F. Lott, Laboratoire de Météorologie Dynamique, Ecole Normale Supérieure, 24 rue Lhomond, 75231 Paris CEDEX 05, France. (flott@lmd.ens.fr)

2169-897X/13/10.1002/jgrd.50705

[5] The major question left open from the 1990s is how to relate the GWs to their potential sources (for an early attempt to include all the sources, see, nevertheless, *Rind et al*. [1988]). This question is more relevant today, because GCMs with stratospheres are now routinely part of the CMIP Earth System Models [*Charlton-Perez et al.*, 2013]: in them, the GW sources do not change when the climate changes. Accordingly, considerable effort have been made over the last 15 years to include nonorographic GWs sources. For instance, *Charron and Manzini* [2002] or *Richter et al.* [2010] have adapted their respective GW schemes to take into account the forcing by fronts. *Beres et al.* [2004] and *Song and Chun* [2005] have proposed formalisms based on monochromatic GW theory to relate the GWs to convection. One problem, if we try to follow these authors, is to decide if it is better to start from a globally spectral scheme (as in *Charron and Manzini* [2002]) or from a multiwave scheme (as in *Beres et al.* [2004]).

[6] To make a decision, we can use the fact that direct observations in the lower stratosphere often show that the GW field is very intermittent, and is often dominated by rather well-defined GW packets [*Hertzog et al.*, 2008]. These observations suggest that the GW vertical spectra observed in the atmosphere are likely to result from ensemble averages of quite narrow-banded periodograms. Also, the balloon observations are quite low in the stratosphere, and not far above the GW sources, which tells that a given source at a given time never realizes the entire GW spectrum. It is therefore quite reasonable to sample the spectrum by launching few monochromatic waves to mimic the quasi monochromatic nature of the observed GW packets, and to choose the GW properties stochastically to mimic the intermittency. This is basically what is done in *Eckermann* [2011], which has adapted the multiwave parameterization summarized in *Garcia et al.* [2007] by launching at each model "physical" time step one monochromatic wave only, the characteristics of the wave being chosen randomly. *Eckermann* [2011] has shown that such a method can be used to correct model biases in the midlatitudes. *Lott et al.* [2012] have shown that it can also be used to help a model to produce a QBO.

[7] One could criticize *Eckermann* [2011]'s approach since each wave has a lifetime that is shorter than the model time step, whereas their period can be much longer, which somehow undermines the WKB assumptions which are at the base of all the GW parameterizations. Nevertheless, this shortcoming is not much worse than other common approach, like the instantaneous vertical propagation of the GW packets, or their horizontal confinements to one grid box area. Also, *Lott et al.* [2012] have shown that this shortcoming is easily corrected by distinguishing the time scale of the GW life cycle from the model time step, and using an order 1 autoregressive (AR1) relation between the GW drag at a given time and that at the next time step. Each GW can now act on a longer time, and at each time, a very large ensemble of waves can act at the same place. More technically, this could help to reduce the production of grid-scale noise, an issue that is not so critical when we look at the global effects of the GWs [*Eckermann*, 2011; *Lott et al.*, 2012], but that could be more significant when we look at the local effects of the GWs breaking [*Lott*, 2003; *Martin and Lott*, 2007]. Finally, it is also important to emphasize that when many waves act at the same time, the scheme can be viewed as a stochastic sampling of a more conventional Fourier series.

[8] In addition to the above motivations, it is worthwhile to recall that there is growing interest in the development of stochastic parameterizations. A first reason is practical and follows from the fact that there is a need to increase the spread of model simulations to produce ensemble predictions [*Shutts*, 2005]. A second reason is may be more fundamental, and follows from the fact that the small scales dynamics at the basis of the subgrid scale parameterizations is not predictable from the large scale environment and is inherently stochastic (see a discussion in *Palmer et al*. [2005]). There is a good example of this in *Doyle et al*. [2011], where even orographic GWs seem to have quite low predictability. The last reason follows from the work by *Piani et al.* [2004] who introduced stochastic effects in the *Hines* [1997]'s parameterization, and found that this helps the model to better simulate the QBO.

[9] The purpose of this paper is therefore to pursue *Lott et al*. [2012] and to relate the GW parameterization used in it to convection. Section 2 describes the formalism, section 3 presents off-line tests using the ERA Interim reanalysis (ERAI) [*Dee et al.*, 2011] for the wind and temperature fields and the Global Precipitation Climatology Project (GPCP) [*Adler et al.*, 2003] for the precipitation. Section 4 presents the impact of the scheme in the LMDz GCM and discusses some sensitivity aspects of the parameterization to the model setup.

2. Formalism

[10] To relate the gravity waves to the convective forcing, we will use the surface precipitation P, because current climate models are tuned to well predict its mean climatologies (for the LMDz model, see *Hourdin et al.* [2006]). Other choices could be made, as, for instance, the vertical profiles of the convective heating predicted by the model, but these still present known biases [*Del Genio et al.*, 2012]. It also seems that the errors in the heatings due to different types of convections (large-scale or parameterized) can compensate to give quite realistic total precipitation (for LMDz, R. Roerhing, private communication, 2013). Also, precipitation is now routinely measured, so schemes keyed on these fields can more easily be tested by others in off-line modes and using global data sets and reanalysis products (as done here in section 3). Also, we will always consider the total precipitation, that is the sum of the large-scale and of the convective precipitation. Again, this is motivated by the fact that the ratio between these two types of precipitations can vary substantially from one model to the other, or when one changes the convection scheme within a given model. More fundamentally, using total precipitation is motivated by the fact that even if a model simulates well the gridscale mean, it remains that in reality this gridscale mean is realized by a large ensemble of small scale clouds. In this case the clouds do not need to be represented by a subgrid scale convection scheme, but can still produce GWs. Of course, there is an issue of how to translate the gridscale mean into subgrid variations, and this calls for a better knowledge of the precipitation spectra. Here we make the hypothesis that this spectra is essentially white.

[11] To translate precipitation into diabatic heating, we distribute the latent heat it produces over a Gaussian distribution in the vertical (as in *Beres et al.* [2004], except that these authors use a bounded sinusoidal function). If we take the thermodynamic equation written in log-pressure coordinate, this yields a tendency on the temperature field given by

$$D_t T + \frac{\kappa T}{H} w = \frac{L_c P}{\rho_0 c_p} \frac{e^{-\frac{(z-z_s)^2}{2\Delta z^2}}}{\Delta z \sqrt{2\pi}}, \tag{1}$$

where z_s is the altitude where the heating is maximal, Δz characterizes the heating source depth, $\rho_0 = \rho_r e^{-z/H}$, where $\rho_r = RT_r/p_r$, T_r and p_r being constant reference values for temperature and pressure. In (1), L_c is the latent heat of condensation, c_p is the heat capacity at constant pressure, $\kappa = (c_p - c_v)/c_p$, and w is the log pressure vertical velocity

$$w = \frac{Dz}{Dt}, \text{ where } z = H \ln\left(\frac{p_r}{p}\right), \text{ and } H = \frac{RT_r}{g}. \tag{2}$$

To evaluate the wave field produced by the subgrid-scale precipitation P', we use the linearized nonrotating hydrostatic equations,

$$\left(\partial_t + \vec{U}\cdot\vec{\nabla}\right)\vec{u}'_H + w'\vec{U}_z = -\vec{\nabla}_H \Phi' , \quad \rho_0\left(\partial_x u' + \partial_y v'\right) + \partial_z\left(\rho_0 w'\right) = 0 , \tag{3}$$

$$\partial_z \Phi' = \frac{RT'}{H} , \text{ and } \left(\partial_t + \vec{U}\cdot\vec{\nabla}\right)\Phi'_z + N^2 w' = \frac{RL_c P'}{\rho_0 H c_p}\frac{e^{-\frac{(z-z_s)^2}{2\Delta z^2}}}{\Delta z\sqrt{2\pi}}. \tag{4}$$

In (3)–(4), $U(z)$, $V(z)$, and $N(z)$ are the zonal wind, the meridional wind, and the Brunt-Vaisala frequency associated with the mean flow, respectively. Still in (3)–(4), u', v', w', and T' are the disturbances for the wind and temperature produced by the disturbance precipitation P'.

[12] To estimate the wave field, we then follow *Lott et al.* [2012] and represent it with the stochastic series,

$$(u', v', w', \Phi') = \sum_1^\infty C_n \left(\hat{u}_n, \hat{v}_n, \hat{w}_n, \hat{\Phi}_n\right) e^{z/2H} e^{i\left(\vec{k}_n\cdot\vec{x} - \omega_n t\right)},$$
$$\text{where } \sum_1^\infty C_n^2 = 1. \tag{5}$$

Here the C_n's are normalization coefficients that generalize the intermittency coefficients in *Alexander and Dunkerton* [1999], and that correspond to the probability that the wave field is given by its realization w'_n. This interpretation permits to treat each GW independently from the others, but neglect the nonlinear interactions between the GWs. This approximation is probably adapted to treat critical levels since linear theory predicts quite well what occurs near them. As said in the introduction, this is a more questionable approximation when the GWs break far from critical levels, because this is a very nonlinear process. In the following, we will follow *Lott et al.* [2012], and randomly choose the horizontal wave numbers k_n, l_n, and the frequency ω_n, but will estimate the wave amplitude by applying this formalism to the precipitation field,

$$P' = \sum_1^\infty C_n \hat{P}_n e^{i\left(\vec{k}_n\cdot\vec{x} - \omega_n t\right)}. \tag{6}$$

For the $\hat{P}_n$, we take $\hat{P}_n = P$, which means that (i) the standard deviation of the subgrid scale precipitation P' equals in amplitude the total precipitation P and (ii) that the subgrid-scale variance of precipitations is uniformly distributed over each harmonic. This last assumption is equivalent to consider that the precipitation spectra is white.

[13] To estimate the wave, we then use the vertical velocity equation,

$$\hat{w}_{zz} + \underbrace{\left(\frac{|\vec{k}|^2 N^2}{\Omega^2} + \frac{\vec{k}\left(\vec{U}_{zz} + \vec{U}_z/H\right)}{\Omega} - \frac{1}{4H^2}\right)}_{Q(z)}\hat{w} = \underbrace{\frac{|\vec{k}|^2}{\Omega^2}\frac{RL_c\hat{P}}{\rho_r H c_p}}_{\hat{J}} \frac{e^{-\frac{(z-z_s)^2}{2\Delta z^2} - z/2H}}{\Delta z\sqrt{2\pi}} \tag{7}$$

where $\Omega = \omega - \vec{k}\cdot\vec{U}$ is the intrinsic frequency, and $Q(z)$ is the scorer parameter. In (7), $\hat{J}$ is introduced and the n indices have been dropped to simplify notations. Far above the source, and when N^2 and U are constant, an exact integration of (7) when there is total reflection at $z = 0$ gives,

$$\hat{w}(z) = i\frac{\hat{J}}{2m} e^{-z_s/2H + \Delta z^2/4H^2} e^{-m^2\Delta z^2} e^{im(z-z_s)}, \text{ where } m = \frac{N|\vec{k}|}{\Omega}, \tag{8}$$

and where we have also taken the Boussinesq and hydrostatic approximations of $Q(z)$: $Q \approx N^2|\vec{k}|^2/\Omega^2$. From this equation, and collecting all the factors related to the mathematical shape of the heating into a single tuning parameter of order 1, G_{uw0}, we take for the launched EP-flux,

$$\vec{F}_l^z = \rho_r G_{uw0}\frac{\vec{k}}{|\vec{k}|}\left(\frac{RL_W}{\rho_r H c_p}\right)^2 \frac{|\vec{k}|^2 e^{-m^2\Delta z^2}}{N\Omega^3}\hat{P}\hat{P}^*, \tag{9}$$

where the EP-flux is defined by the relation,

$$\vec{F}^z(k,l,\omega) = \Re\left\{\rho_r \vec{\hat{u}}\hat{w}^*\right\} = \rho_r \frac{\vec{k}}{|\vec{k}|^2} m(z)|\hat{w}(z)|^2. \tag{10}$$

In (10), the second equality follows a WKB treatment of (7) far from the sources. In our parameterization, we will start from a launching altitude z_l and impose (9) there and everywhere below.

[14] To move from one model level to the next model level above, we essentially conserve the EP-flux but allow a small diffusivity, $\nu = \mu/\rho_0$, which can be simply included by replacing Ω by $\Omega + i\nu m^2$ and by taking into account that in this case the vertical wave number is also imaginary. This small diffusivity is here to guarantee that the waves are ultimately dissipated over the few last model levels, if they have not been before (hence the division by the density ρ_0). We also limit the new EP-flux amplitude to that produced by a saturated monochromatic wave, e.g., a wave of amplitude

$$\hat{w}_s = S_c \frac{\Omega^2}{|\vec{k}|N} e^{-z/2H} k^*/|\vec{k}|, \tag{11}$$

where S_c is another tunable parameter of order 1 and k^* a characteristic horizontal wavelength corresponding to the longest among the waves that one parameterizes. In *Lott et al.* [2012], $k^* = 1/\sqrt{\Delta x \Delta x}$, where Δx and Δy are the horizontal scales that the model cannot well solve explicitly: Δx and Δy can reasonably be well taken for the subgrid scale region corresponding to a GCM grid (δx and δy). Finally, we also annul the EP-flux when we pass through a critical level

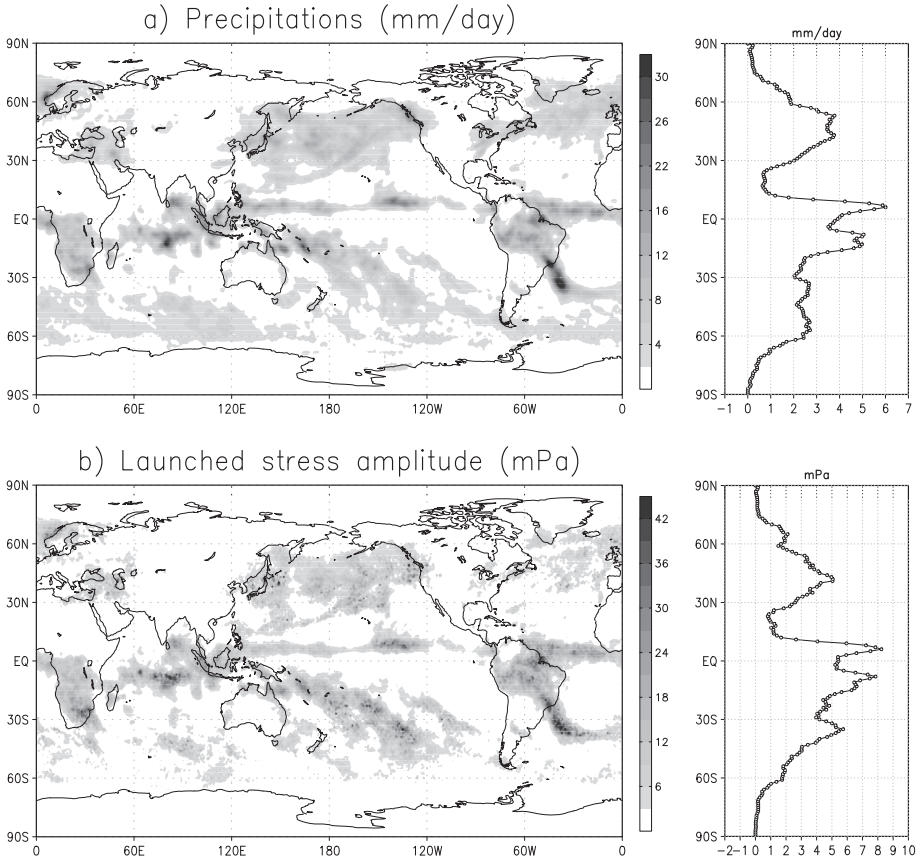

Figure 1. Precipitation and convective GWs stress predicted off-line using the GPCP data set and the ERAI reanalysis. All fields are from daily outputs averaged over the first week of the year 2000. (a) Precipitation and its zonal mean; (b) launched stress amplitude (see equation (15)). In Figures 1a and 1b, the right panels are for the zonal average.

where Ω changes sign. To summarize, the passage from one model to the next can be written,

$$\vec{F}^z(z+\delta z) = \frac{\vec{k}\Omega}{|\vec{k}||\Omega|}\Theta(\Omega(z+\delta z)\Omega(z))) \\ \text{Min}\left\{|\vec{F}^z(z)|e^{-2\frac{\mu m^3}{\rho_0\Omega}\delta z},\ \rho_r S_c^2\frac{|\Omega|^3k^{*2}}{N|\vec{k}|^4}\right\}, \qquad (12)$$

where the first fraction is to guarantee that the EP-flux is in the direction of the phase speed, the second term with the heavyside function $\Theta(z)$ handles critical levels, the first term in the parenthesis express the decay of the EP-flux due to diffusion, and the last term is the saturated EP-flux. Note that when (12) is applied for the first time and at the next level above the launching level z_l, the new value replaces the launched value at all altitudes below. This prevents abrupt change in flux just above z_l and the launching of waves with unrealistically large amplitudes.

[15] To choose the C_n's, we again follow *Lott et al.* [2012] and consider that we need to parameterize GWs whose life cycle is contained in a characteristic time interval Δt. Here it is important to note that Δt has to largely exceed the GCM time step δt, otherwise we would only parameterize very fast waves: the physical time step δt of a GCM is less than an hour, whereas the time scale of the life cycle of the convection that produces the waves can easily be near $\Delta t \approx 1$ day. Accordingly, we launch a few (say M) waves at each time step, and redistribute the tendencies produced at each time step δt over a longer Δt by using the AR1 relation presented in *Lott et al.* [2012]:

$$\left(\frac{\partial\vec{u}}{\partial t}\right)^t_{\text{GWs}} = \frac{\delta t}{\Delta t}\frac{1}{M}\sum_{n'=1}^{M}\frac{1}{\rho_0}\frac{\partial\vec{F}_{n'}}{\partial z} + \frac{\Delta t-\delta t}{\Delta t}\left(\frac{\partial\vec{u}}{\partial t}\right)^{t-\delta t}_{\text{GWs}}. \qquad (13)$$

If we express the cumulative sum underneath the AR-1 relation in (13), we recover the formalism for stochastic waves infinite superposition in (5) by taking

$$C_n^2 = \left(\frac{\Delta t-\delta t}{\Delta t}\right)^p\frac{\delta t}{M\Delta t}, \qquad (14)$$

where p is the nearest integer that rounds $(n-1)/M$ toward the left.

3. Off-Line Tests

3.1. Data Sets and Parameters Values

[16] To save computer time during the tuning of the scheme, and to use data sets that are shared worldwide so that our results can be reproduced by others, we have developed an off-line environment. As input, it uses the winds and temperature from ERAI and precipitation from GPCP [*Adler*

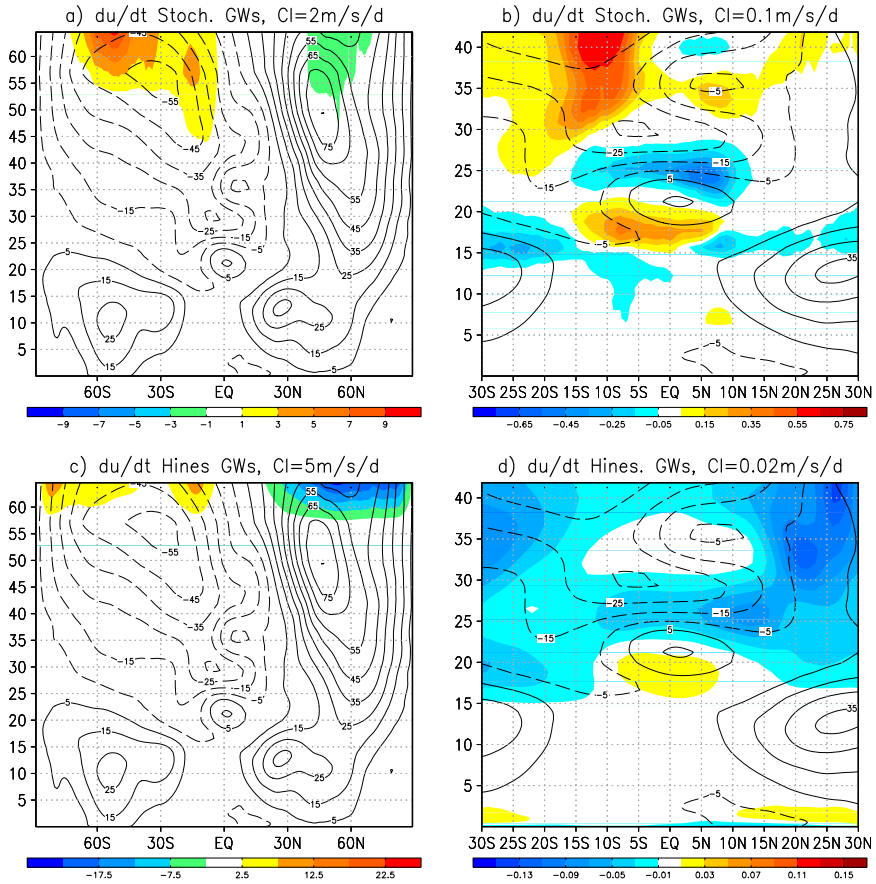

Figure 2. Zonal and temporal mean values of the nonorographic gravity waves drag (in m/s/day, shaded) and of the zonal mean zonal wind (in m/s, continuous and dashed lines) for the same periods and data sets as in Figure 1.

et al., 2003]. As the GPCP data set is for daily products at the horizontal resolution of $1^o \times 1^o$, we use the ERAI products at the same resolution, and on the 60 ERAI model levels which go up to around 65 km (10 Pa), with a resolution in the stratosphere around 1–2 km. For the horizontal resolution, we will see in section 4 that it is much more refined than the horizontal resolution of our GCM, but that the temporal resolution of 1 day is much larger than the GCM physical time step δt = 30 min. We could have interpolated the grid of the data sets to match that of the model, but this is not well justified, since in the end, all the results of interest are conventionally normalized by the grid surface areas and averaged in time.

[17] Concerning the scheme itself, the parameters chosen are G_{uw0} = 2.4 for the GWs amplitude in (9), S_c = 0.25 for the parameter controlling the breaking in (11), and μ = 1 kg m^{-1} s^{-1} for the dissipation parameter controlling the decay of the EP flux in (12). Also, we have limited the spectral precipitation rates $\hat{P}_n$ that enter in the launching flux (9) by a maximum value of P_M = 20 kg m^{-2} day^{-1} and using a smooth tanh transition (e.g., by replacing the harmonic amplitude $\hat{P}_n = P$ by $\hat{P}_n = P_M \tanh(P/P_M)$). This choice is motivated by the fact that our linear GW theory is not very well adapted when there are large precipitations, and we have considered that in these cases, the theory overestimates the waves amplitude. Also, we have considered that for a given harmonic, the source vertical scale Δz = 1 km in (1), which ensures that the heating is distributed in the vertical over around 5 km, which is essentially in agreement with observations [*Del Genio et al.*, 2012]. Although we will not discuss this further, it is important to emphasize here that the scheme can be very sensitive to the parameter Δz. From equation (9), we can show that the launching flux varies in $m^3 e^{-m^2 \Delta z^2}$ for a given precipitation, so there is a relative maximum in the flux for a vertical wavelength near $m \approx \Delta z^{-1}$. From the dispersion relation in (8), this corresponds to phase speeds around $C \approx N\Delta z \approx 10$ m/s for the value of Δz = 1 km we have chosen. A smaller Δz would make the total flux larger but transported by slower waves and the other way round. Our choice here is therefore a compromise and further work might be needed to constrain better this quantity. Also, we have considered that the source is centered in the midtroposphere at z_s = 500 hPa, that this level is the launching altitude, and evaluated all the large scale flow tropospheric parameters that enter in the launching flux in (9) by averaging the winds and the Brunt-Vaisala frequency between the ground and a characteristic cloud top max altitude of 200 hPa.

[18] To specify the wave characteristics, we follow *Lott et al.* [2012] and choose randomly the waves absolute phase speed between $C_m < C = |\omega/k| < C_M$ where C_m = 1 m/s and C_M = 50 m/s, and the horizontal wave number between $k^* < |k| < k_s$ with k_s = 1 km^{-1} and k^* = 0.02 km^{-1} (this last choice for k^* assume that the waves with scale below around

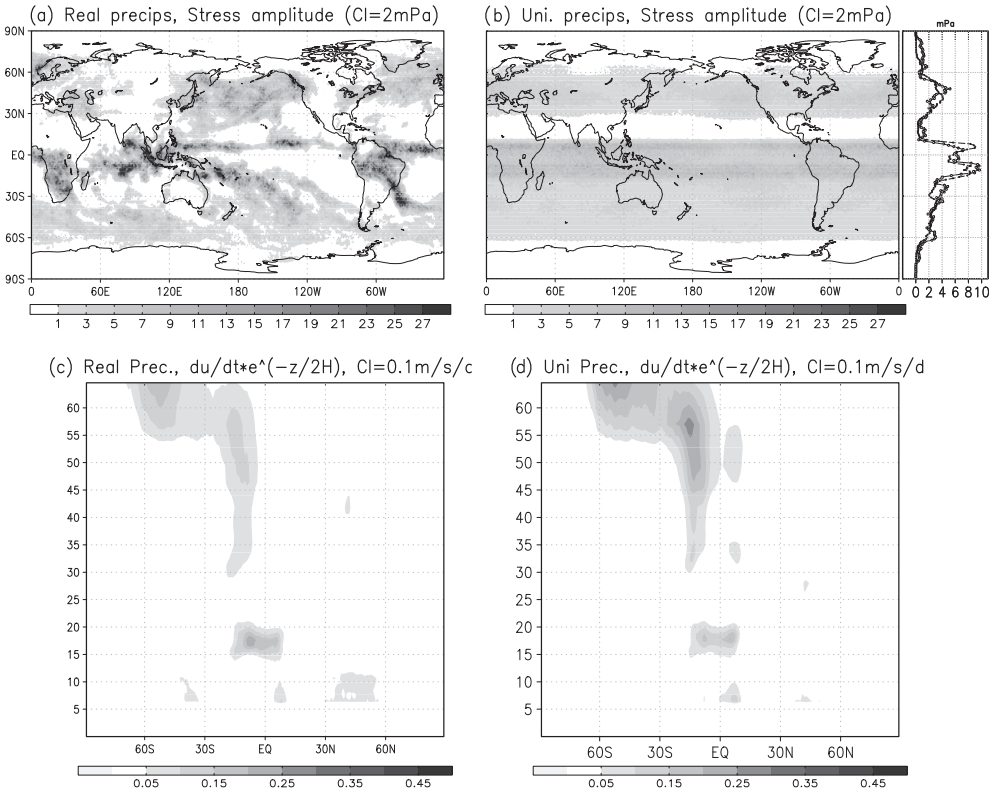

Figure 3. GWs stress and drag due to waves with positive phase speed, same data as in Figures 1. (a) Stress magnitude, (b) stress magnitude when precipitations are averaged in longitude and time over the 7 day period, (c) gravity wave drag associated with the stress in Figure 3a; (d) GWD associated with the stress in Figure 3b. In Figures 3c and 3d, the tendencies are scaled by $e^{-z/2H}$ to display on the same panel the tendencies acting in the low stratosphere and those acting near and above the stratopause.

300 km still need to be parameterized, an assumption that is adapted to our GCM). Finally, in all these random choices, the probability density between the bounds given is constant, we launch $M = 8$ waves by day per grid point, and we only consider eastward moving and westward moving GWs.

3.2. Results

[19] Figure 1a presents the GPCP mean precipitations averaged over the first week in 2000, and Figure 1b, the absolute momentum flux carried by the convective GWs,

$$\frac{1}{56}\sum_{d=1}^{d=7}\sum_{m=1}^{m=8}|\vec{F}_m^z(d,\lambda,\phi,z_l)|, \qquad (15)$$

where d, λ, and ϕ are the day, the latitude, and the longitude, respectively. The first notable result in Figure 1b is that the regional variations of the GW stress are very pronounced, with regions where it can approach 50 mPa and more. These correspond to regions of intense precipitation as shown in Figure 1a. Thus, much of the GW stress emerges from the ITCZ and SPCZ, as well as from the midlatitude NH winter storm tracks over the Atlantic and Pacific oceans. The zonal average of the GW stress amplitude on the right of Figures 1a and 1b show well these different regions of GW production, with more waves coming from the equator and tropics. This can be potentially helpful for the LMDz-GCM, since we know from *Lott et al.* [2012] that enhanced GWs in these regions can produce a QBO in this model.

[20] The temporal and zonal average of the drag produced by the convective GWs and over the same period is shown in Figures 2a and 2b. Figure 2a shows that the scheme applies a substantial drag near the reanalysis top, that is, a drag comparable to the drag produced by the *Hines* [1997] parameterization currently operational in LMDz (Figure 2c). Also, the convective GW drag is quite substantial and positive near the model top in the southern hemisphere midlatitude and subtropical regions, where it can significantly add up to the drag produced by the *Hines* [1997]'s scheme. In this sector, we know from *Lott et al.* [2005] that LMDz have large easterly biases, and we will see in section 4.3 that this extra drag can help to improve the model climatology there.

[21] The zoom over the low stratosphere and equatorial regions in Figure 2b) shows that the scheme applies a drag with maximum value around 0.3 m/s/d about 1–2 km below where the jet is maximum in the QBO region around 20 km, and a negative drag in the strongly and negatively sheared region centered at $z = 25$ km. From *Giorgetta et al.* [2006], we know that such values can produce a QBO in a GCM with sufficient vertical resolution. The same zoom for the GW drag due to *Hines* [1997] in Figure 2d shows maxima and minima at about the same place as in Figure 2b but with amplitudes around 10 times smaller. Clearly, the setup adopted for the *Hines* [1997]'s scheme to improve the

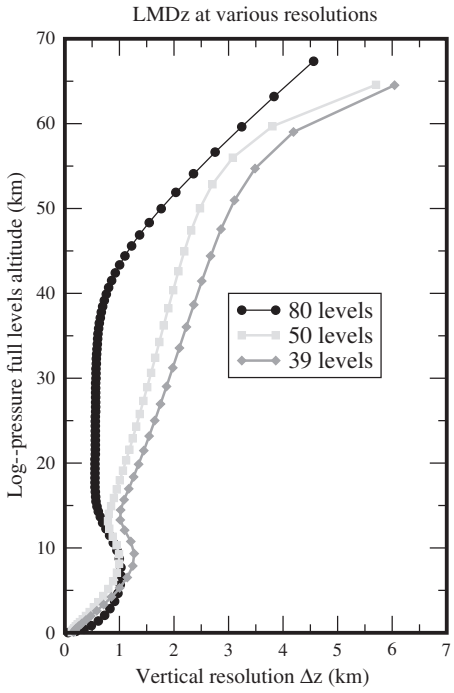

Figure 4. Log-altitude of the vertical levels used in LMDz and defined as $z_l = 7\ln(p_r/p_l)$, where $p_r = 1013$ mb, and p_l is the model level pressure. The grid is compared to other versions with stratosphere, like the 50 level version coupled to stratospheric chemistry in *Jourdain et al.* [2008] or the 39 level version used in CMIP5 [*Maury et al.*, 2013].

midlatitudes in *Lott et al.* [2005] does not result in enough drag in the tropical regions. For completeness, note nevertheless that there are setups for the *Hines*'s [1997] scheme that can make it more efficient in the QBO region [*Giorgetta et al.*, 2006].

[22] One consequence of relating the GWs to their convective sources by our method, is that the zonal mean stress in Figure 1b, (right) results from quite few large amplitude GWs (see Figure 1b, left). It is likely that for a comparable averaged stress, these few GWs of large amplitude break at lower altitudes than would a much larger ensemble of waves with more uniformly distributed amplitudes. This can help a GWs scheme to be more efficient in the QBO region, without yielding very large drags at higher altitudes, like, for instance, in the region of the SAO.

[23] In the off-line setup, this idea can be tested by averaging the precipitations in time and longitude and by using these averaged values in the launching stress (9). The result for the stress amplitude due to the waves with positive phase speed is shown in Figure 3b. When we compare it to the stress produced by the real precipitation field in Figure 3a, we see that it is much more uniformly distributed. Nevertheless, the zonal mean values stay comparable, as shown in Figure 3b, right. The corresponding drags are displayed in Figures 3c and 3d, where we see that uniform and nonuniform precipitations produce quite equivalent effects in the QBO region. Near and above the stratopause, however, we see that when the sources are much more sporadic, the zonal mean drag is smaller than when the sources are more uniform.

4. Online Simulations

4.1. Model Description

[24] To test the parameterization online, we take the version of LMDz described in *Lott et al.* [2012]. In the horizontal, the grid is $1.875° \times 3.75°$ in latitude and longitude, respectively and, in the vertical, the model has 80 levels, with the model top near $z = 65$ km, and with a vertical resolution around 600 m between $z = 15$ km and $z = 35$ km (see Figure 4, where the vertical resolution is compared to other operational versions of LMDz). For the convective GWs scheme, the online setup is as in section 3, except that we now launch $M = 8$ waves per grid point each physical time step $\delta t = 30$ min instead of each day. It means that around $M \times \Delta t/\delta t \approx 400$ stochastic harmonics contribute to the wave field each day and at a given horizontal grid point. This very large sample of waves acting at a given place is clearly a major benefit of the scheme. Finally, we keep the *Hines* [1997] nonorographic GW drag scheme and the *Lott* [1999] orographic parameterization scheme, which have been tuned to give a realistic midlatitudes climate in the stratosphere [*Lott et al.*, 2005], and we will check in section 4.3 that the new scheme is not detrimental to the midlatitudes. Concerning the horizontal diffusion and by comparison with *Lott et al.* [2005], the decay time scale of the smallest divergent modes has been left to 1 h, but that on the smallest vortical modes has been increased from 1.5 to 6 h. With these choices, the QBO winds are less dissipated, because they are nondivergent, but the external gravity waves that controls the numerical stability of the model are dissipated as before. Finally, all the simulations presented in this paper are forced by climatological surface fields of sea surface temperature, soil temperature, and composition over land, and the length of the simulation presented next is 85 years.

4.2. QBO Structure

[25] The results for the zonal wind at the equator in Figure 5a show that the model simulates a QBO. It has an amplitude of around 15–20 m/s at 10 hPa, that is smaller than the 20–25 m/s amplitude displayed in Figure 5b. The easterly phases are also stronger than the westerly phases by about 20 m/s, this is slightly more than the observations, where this difference is around 10–15 m/s. Also, in the model, the westerly phases have a shorter duration than the easterly ones, which is consistent with the observations. In the middle stratosphere between 10 and 1 hPa, the QBO in the model seems quite disconnected from the SAO, in the sense that there is no clear connection between the onset of similar phases in the two oscillations in this sector. This is particularly true if we look at the westerly phase of the SAO, and quite in contradiction with the observational results in *Dunkerton and Delisi* [1997]. In fact, these authors have shown that the westerly phases of the SAO contribute to the descent in the stratosphere of the westerly phase of the QBO, an effect that is clearly absent in our model, but that can be found in the reanalysis, and especially the MERRA reanalysis in Figure 5b. Note that we show two reanalysis here because we know that they are significantly different in the low equatorial mesosphere, a place where there is little observational constraint (see *Rienecker et al.* [2011], who also discuss the fact that in the low equatorial stratosphere, the QBO is realistic in both MERRA and ERAI).

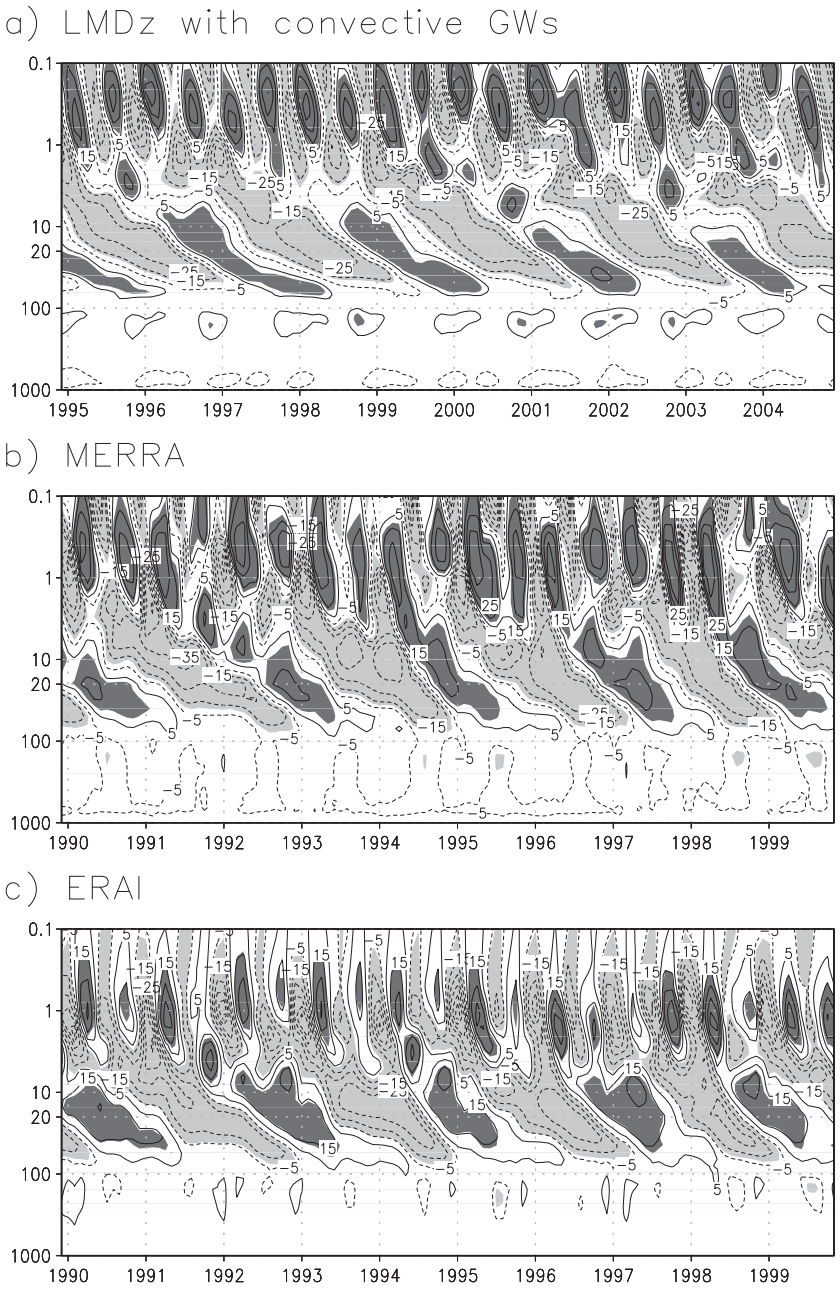

Figure 5. Zonal mean zonal wind averaged over the equatorial band 5°S–5°N, (a) LMDz with 80 levels and the convective waves parameterization; (b) MERRA reanalysis; (c) ERAI reanalysis. Contour interval: 10 m/s, values above and below ± 10 m s^{-1} dark grey shaded and light grey shaded, respectively.

[26] The histograms of the period of the QBO cycles in LMDz are shown in Figure 6 and compared to those obtained from the observed QBO data set described in *Naujokat* [1986], and which is today 50 years long (1953–2012, see the Freie Universitat of Berlin website). In both data sets, the period of the QBO is determined as the difference between the dates when the zonal mean zonal wind at the equator and at 40 hPa changes from easterlies to westerlies. In the model, the averaged QBO period is near 26 months, that is 2 months shorter than in the observations, and can take values between 23 and 30 months. Although the spread of periods is quite substantial, it is nevertheless less important than that found in reality, and despite the fact that the observational period is shorter in duration (50 years for 19 QBO cycle) than the simulated one (85 years for 39 QBO cycles). Compared to *Lott et al.* [2012] where the oscillation was purely biennial, we have now completely unlocked the QBO from the annual cycle. Also, and since the periods do not show preferences to be near multiples of 6 months, the histogram results confirmed that our QBO is not much triggered by the SAO. In this respect, our simulation of the QBO is quite different than others, like, for instance, the Met Office Unified Model simulation in *Scaife et al.* [2002], where the QBO periods cluster around 24 and 30 months, and where the SAO-QBO relation described in *Dunkerton and Delisi* [1997] is probably too well preserved.

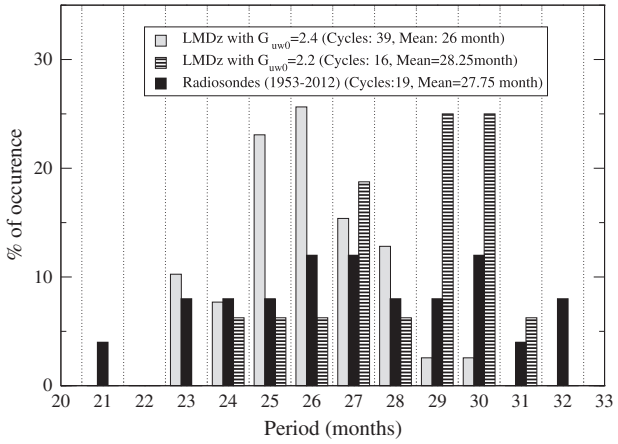

Figure 6. Histogram statistics of the QBO period in LMDz and compared with radiosondes, both at 40 hPa. The period is taken as the time between easterly and westerly wind transitions, and the radiosondes data are taken from the Freie Universitat of Berlin website.

[27] The meridional structure of the model QBO is shown in Figure 7, which presents composites of the zonal winds keyed to extrema of the zonal wind at the Equator at 20 hPa. Here we only compare to ERAI and after verification that the composites from MERRA are almost identical. In the model, the westerly jet at 20 hPa in Figure 7a is deeper in vertical extent than the easterly jet in Figure 7b, and this is somehow consistent with the reanalysis in Figures 7c–7d. Note nevertheless that in the reanalysis, these jets are deeper in vertical extent than in the model. In the reanalysis also, the westerly jet in Figure 7c is broader in latitude than the easterly jet in Figure 7d. This asymmetry in meridional extent is almost absent from the model, where the QBO also seems to be too confined to the equator.

[28] To relate our online results here to the off-line calculations done in section 3, the Figures 8a and 8b present the precipitation fields and the stress launched by the stochastic GWs scheme averaged over one given week in January. When we compare to Figure 1, we see a strong resemblance, once taken into account that the model resolution is much coarser than the observational data sets used in Figures 1a and 1b. In particular, and because our model has a quite realistic precipitation climatology (compare for instance Figure 1a, right and that in Figure 8a, right) the spatial distribution and the zonal average of the convective GWs stress amplitude in the model compare well with those predicted with the observations. We also find that the stochastic GWs are much more efficient than the *Hines* [1997] scheme in the QBO region, but much less near the model top (not shown, but this is as expected from section 3). As expected also, the convective GWs nevertheless tend to apply a positive drag in the summer subtropical mesosphere, a place where our configuration of the *Hines* [1997]'s scheme is not very effective.

4.3. Other Impacts and Sensitivity Tests

[29] As the stochastic GWs scheme exerts substantial drags at higher altitudes than the QBO regions and also in the subtropics and midlatitude summer mesosphere, we have to verify that it does not degrade the SAO and the climatological zonal mean zonal winds.

[30] To analyze the SAO, the Figures 9a–9d present the annual cycle of zonal winds for the MERRA reanalysis, the ERAI reanalysis, the LMDz simulation with the convective GWs, and the LMDz simulation without. When we

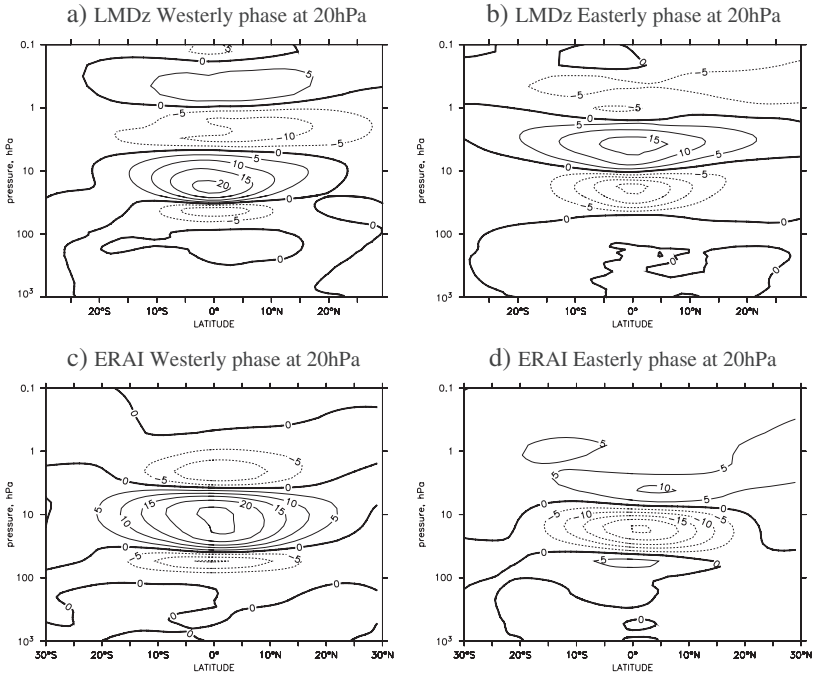

Figure 7. Composite of the zonal mean zonal wind when the QBO phase is such that the zonal mean zonal wind reaches an extreme value at 20 hPa and after substraction of the annual cycle.

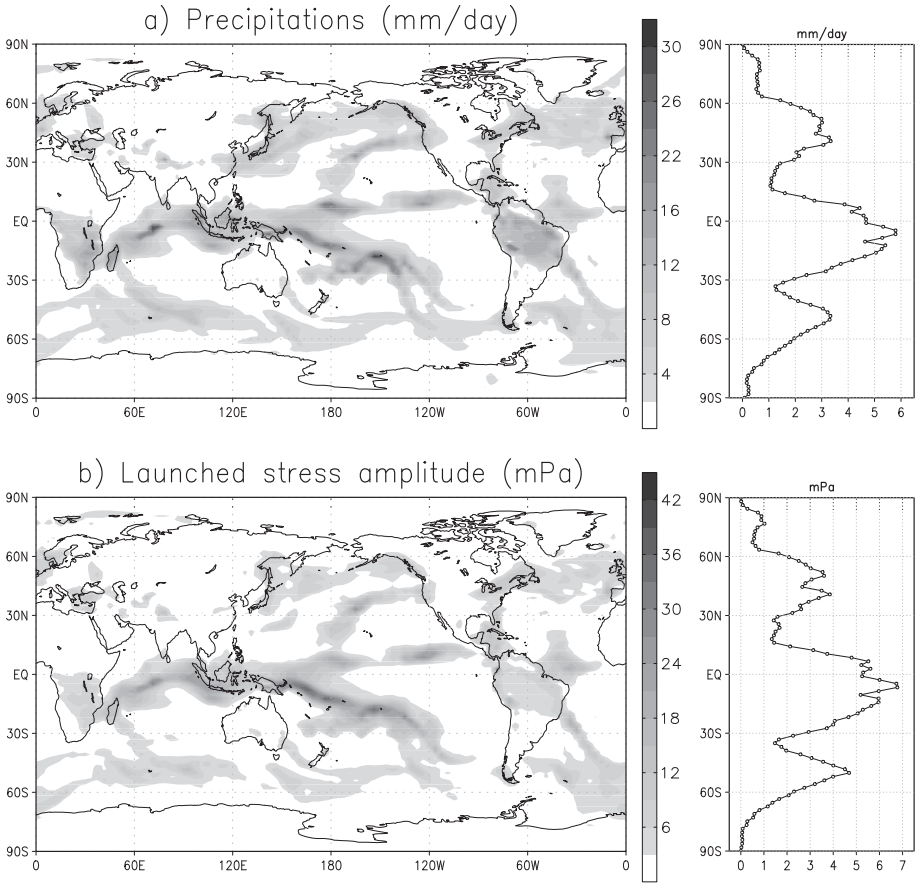

Figure 8. Same as Figure 1 but online and for the first week of the 82nd year of the LMDz control simulation.

compare the two model results with the reanalysis, we see that in the model, the SAO never descends down to 10 hPa and even below as it does in MERRA. Also, a quite remarkable error in the simulation without GWs in Figure 9d, is that the maximum of westerly wind is in October, rather than being in March–April. When the GWs scheme is activated in Figure 9c, this error is corrected, and the overall descent of the SAO signal slightly improved. Such a positive impact

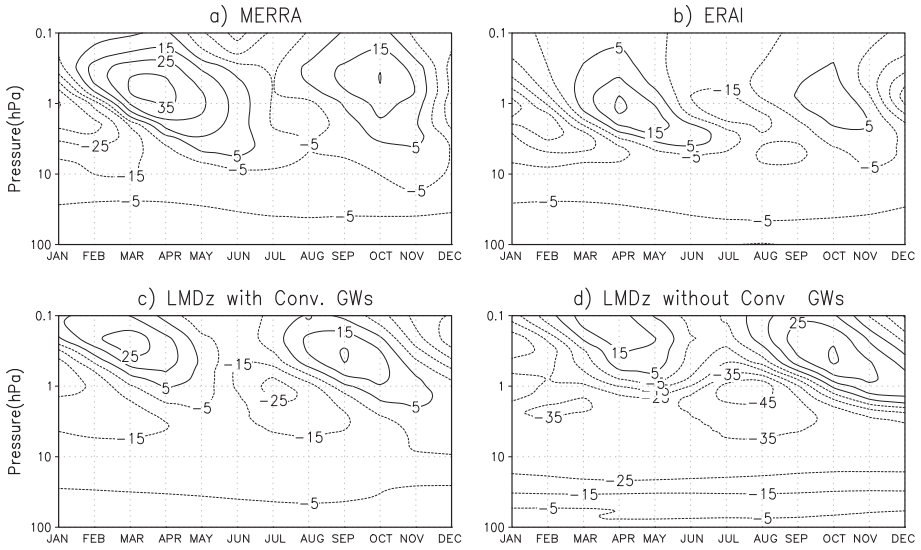

Figure 9. Annual cycle of the zonal mean zonal wind averaged over the equatorial band 5°S–5°N: (a) MERRA reanalysis; (b) ERAI reanalysis; (c) LMDz with 80 levels and the convective GWs parameterization; (d) LMDz with 80 levels and without the convective GWs parameterization.

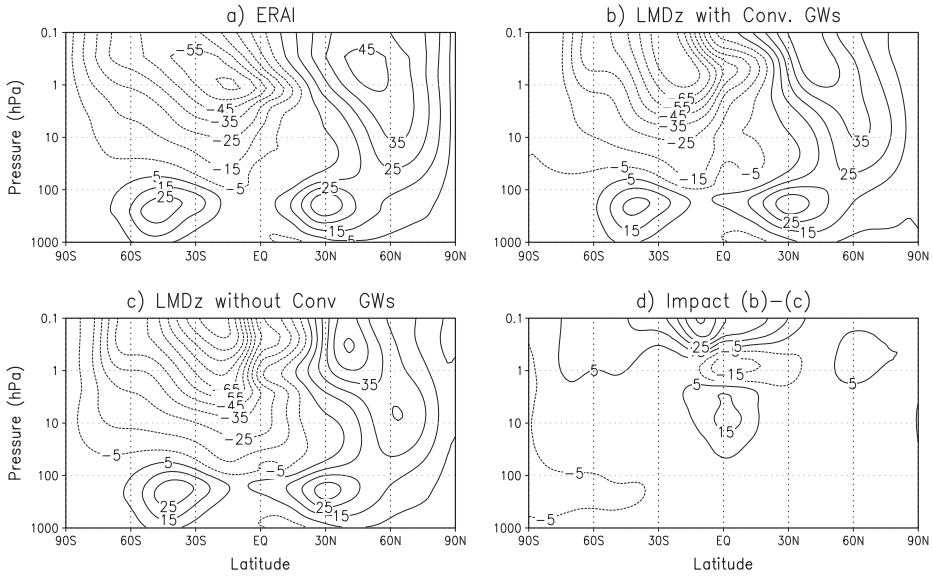

Figure 10. January climatologies of zonal wind. (a) ERAI reanalysis; (b) LMDz with 80 levels and the convective GWs parameterization; (c) LMDz with 80 levels and without the convective GWs parameterization; (d) difference between Figures 10b and 10c.

of convective GWs on the SAO was also reported in *Song et al*. [2007].

[31] To measure the impact of the scheme in other places than just the equatorial regions, Figure 10 shows the zonal mean zonal wind January climatology from the model with and without the stochastic GWs scheme. Overall, the major differences stay indeed confined to the equator with a very substantial improvement in the QBO and SAO regions around and above 1 hPa typically. Above that level, and in the summer mesosphere subtropics, the scheme also yields to a substantial reduction of the easterlies amplitude. Nevertheless, at this altitude, we know from *Lott et al.* [2005] that the model has an easterly bias. This bias is apparent in Figure 10c near above 10 hPa and around the latitudes 30°S–20°S where the easterlies in the model without convective GWs reach almost –100 m/s, instead of around –70 m/s in ERAI. This error is substantially reduced with the convective GWs scheme which supports the suggestion that our model can support extra GWs drag in these subtropical summer regions. In the midlatitudes and polar regions, the impact of the scheme stays moderated, and we have of course verified that comparable changes occur for the other months.

[32] As others, we have also tested the effect of the horizontal diffusion in our model [see, e.g., *Takahashi*, 1999; *Scaife et al.*, 2002], but have adopted a different approach. As said at the beginning of section 4.1, and compared to *Lott et al.* [2005], we have increased the timescale of decay of the smallest vortical modes to 6 h and left unchanged that of the divergent modes. We have argued that this decreases the numerical damping of the QBO without destabilizing the model, simply because the stability is controlled by the external (divergent) gravity waves. Therefore, and to illustrate that the dissipation of the vortical mode only affects the QBO period, we have decreased its timescale to 3 h instead of 6 r, and left that on the divergent modes unchanged. We found that this decreases the QBO period of around 2–3 months. We have also tested many different nonorographic GWs setup and found without surprise that these affect the QBO period significantly. For instance, without the *Hines* [1997] scheme the QBO period increases by around 2 months. As our QBO period is also quite short, we have also made a long test with a GWs launching amplitude reduced to G_{uw0} = 2.2 (see equation (9)). This increases the QBO mean period to 28.25 months, and does not seem to affect the spread of periods (see Figure 6).

5. Conclusion and Discussion

[33] A parameterization of convectively generated gravity waves is proposed, which treats the large spectrum of gravity waves due to convection by the stochastic approach presented in *Eckermann* [2011]. As this stochastic approach is formally very close to a more conventional Fourier analysis of the wave field, it can include source terms by using the linear theory of GWs forced by convection, as done for instance in *Beres et al.* [2004] or *Song and Chun* [2005]. As stochastic approaches can be used to bin almost continuously a very large spectrum of gravity waves [see *Lott et al.*, 2012], they have the potential to treat very efficiently the long-term effects of gravity waves critical level interactions, a process that is known to be significant for the QBO dynamics.

[34] First, the scheme is tested off-line and by using fields from the ERAI reanalysis and from the GPCP precipitation data set. In this setup, we find that for the routine setup that will be used online, the scheme produces very sporadic gravity waves fluxes, following the sporadic nature of convection. In terms of zonal mean effects, nevertheless, the parameterized GWs give tendencies that compare well, in the QBO region, to the characteristic tendencies needed to produce the QBO. Also, these off-line tests show that the strong intermittency introduced by convection make the GWs deposit momentum at lower altitudes than when the

sources are more uniform. Importantly, the results of these off-line tests translate very well online, which means that off-line techniques can become very powerful, since they can be used during field campaigns like Vorcore [*Hertzog et al.*, 2008] or to interpret satellite measurements [*Alexander et al.*, 2010].

[35] Second, the scheme is tested online, using the stratosphere resolving LMDz model with 80 vertical levels presented in *Lott et al.* [2012] but where statistically uniform sources of GWs were imposed in the tropical regions. As in *Lott et al.* [2012], we find that the scheme can produce a QBO in the model, with the additional effect that the QBO now has an irregular period around 27 months, and that is no longer strictly keyed to the annual cycle (in *Lott et al.* [2012], the QBO period is 24 months exactly). To our knowledge, this is the second example in the literature of a model producing a QBO, including GWs that are explicitly related to their convective source (see the recent paper by *Kim et al.* [2013]). We think that part of this success comes from the fact that (i) our stochastic treatment of the gravity waves permits us to develop a fully spectral scheme at a minimal numerical cost, and that (ii) the relation with the very sporadic convective sources allows our waves to be efficient at low altitude without degrading the model performance at higher levels.

[36] Apart from that, the model QBO has some errors: it is slightly too confined in the tropical region, its amplitude is around 10% smaller than in the observations, and the vertical scale over which it changes sign is slightly too short. We think that these errors do not have to be corrected by the GWs only, since other studies indicate that the LMDz model lacks planetary scale equatorial waves [*Maury et al.*, 2013]. These studies also suggest that the GWs in our model probably play a slightly excessive role in the QBO forcing when compared to that of Kelvin waves, for instance.

[37] Although our scheme permits us to treat a large ensemble of waves, it has the defect of the other multiwave scheme of treating the breaking of each wave independently from the others. Although this contradicts the fact that breaking is a nonlinear process, it should be kept in mind that in the QBO region, a lot of the wave-mean flow interactions occur near critical levels, a mechanism that is well predicted via the linear theory [*Lott and Teitelbaum*, 1992]. At higher altitude, and when breaking occurs away from critical levels, the globally spectral schemes, like, for instance, *Warner and McIntyre* [1996], might be more realistic since they force the GWs to follow observed saturated spectra. Nevertheless, the globally spectral schemes have the defect of producing full spectra at each time step whereas in reality, a spectrum is an average over a large ensemble of periodograms, each corresponding to individual realizations. So, when we link the GWs to their individual sources, we consider realizations and we can not impose the entire spectra.

[38] Instead of comparing the pros and cons of each approach, it would be more constructive in the near future to see how they could be reconciled. One possible way to do so, is to note that some stochastic WKB theory of GWs can potentially yield vertical spectra resembling those measured [*Souprayen et al.*, 2001]. If true, it means that stochastic techniques like the one used in this paper could be adapted to produce realistic spectra. This could help to improve the realism of some of the random choices we have made in this paper. One of these choices is probably quite critical, it is the assumption that the subgrid scale precipitation spectra is white. As we have seen, this is very convenient, since it justifies that we take the grid scale precipitation amplitude for the amplitude of each subgrid scale precipitation harmonics, but it certainly needs to be much more refined. This spectral tuning of the scheme could also guide further our choices of other critical parameters like the depth of the convective heating (Δz) in (1). Interestingly, we have shown that these issues can, in good part, be treated off-line.

[39] **Acknowledgments.** We thank Elisa Manzini, Richard Lindzen, and Charles Mc Landress for helpful discussions and feedbacks. We also thank two anonymous reviewers for their careful readings and comments. GPCP Precipitation data are provided by the NOAA/OAR/ESRL PSD, Boulder, Colorado, USA, from their Web site at http://www.esrl.noaa.gov/psd/. This work was supported by the European Commission's 7th Framework Programme, under the projects EMBRACE (grant agreement 282672) and COMBINE (grant agreement 226520) and by the French ANR agency under the project STRADYVARIUS.

References

Adler, R. F., et al. (2003), The Version 2 Global Precipitation Climatology Project (GPCP) monthly precipitation analysis (1979–present), *J. Hydrometeorol.*, *4*, 1147–1167.

Alexander, M. J., and T. J. Dunkerton (1999), A spectral parameterization of mean-flow forcing due to breaking gravity waves, *J. Atmos. Sci.*, *56*, 4167–4182.

Alexander, M. J., et al. (2010), Recent developments in gravity-wave effects in climate models and the global distribution of gravity-wave momentum flux from observations and models, *Q. J. R. Meteorolog. Soc.*, *136*, 1103–1124.

Beres, J. H., M. J. Alexander, and J. R. Holton (2004), A method of specifying the gravity wave spectrum above convection based on latent heating properties and background wind, *J. Atmos. Sci.*, *61*, 324–337.

Charlton-Perez, A. J., et al. (2013), On the lack of stratospheric dynamical variability in low-top versions of the CMIP5 models, *J. Geophys. Res. Atmos.*, *118*(6), 2494–2505, doi:10.1002/jgrd.50125.

Charron, M., and E. Manzini (2002), Gravity waves from fronts: Parameterization and middle atmosphere response in a general circulation model, *J. Atmos. Sci.*, *59*, 923–941.

Dee, D. P., et al. (2011), The ERA-Interim reanalysis: Configuration and performance of the data assimilation system, *Q. J. R. Meteorolog. Soc.*, *137*, 553–597, doi:10.1002/qj.828.

Del Genio, A. D., J. Wu, and Y. Chen (2012), Characteristics of mesoscale organization in WRF simulations of convection during TWP-ICE, *J. Clim.*, *25*, 5666–5688, doi:10.1175/JCLI-D-11-00422.1.

Doyle, J. D., et al. (2011), An intercomparison of T-REX mountain-wave simulations and implications for mesoscale predictability, *Mon. Wea. Rev.*, *139*, 2811–2831, doi:10.1175/MWR-D-10-05042.1.

Dunkerton, T. J. (1982), Stochastic parameterization of gravity-wave stresses, *J. Atmos. Sci.*, *39*, 1711–1725.

Dunkerton, T. J. (1997), The role of gravity waves in the quasi-biennial oscillation, *J. Geophys. Res.*, *102*, 26,053–26,076.

Dunkerton, T., and D. Delisi (1997), Interaction of the quasi-biennial oscillation and stratopause semiannual oscillation, *J. Geophys. Res.*, *102* (D22), 26,107–26,116, doi:10.1029/96JD03678.

Eckermann, S. D. (2011), Explicitly stochastic parameterization of nonorographic gravity wave drag, *J. Atmos. Sci.*, *68*, 1749–1765.

Garcia, R. R., D. R. Marsh, D. E. Kinnison, B. A. Boville, and F. Sassi (2007), Simulation of secular trends in the middle atmosphere, 1950–2003, *J. Geophys. Res.*, *112*, D09301, doi:10.1029/2006JD007485.

Giorgetta, M. A., E. Manzini, E. Roeckner, M. Esch, and L. Bengston (2006), Climatology and forcing of the quasi-biennial oscillation in the MECHAM5 model, *J. Clim.*, *19*, 3882–3901.

Hertzog, A., G. Boccara, R. A. Vincent, F. Vial, and P. Cocquerez (2008), Estimation of gravity wave momentum flux and phase speeds from quasi-Lagrangian stratospheric balloon flights. Part II: Results from the Vorcore campaign in Antarctica, *J. Atmos. Sci.*, *65*, 3056–3070.

Hines, C. O. (1997), Doppler spread parameterization of gravity wave momentum deposition in the middle atmosphere. Part 2. Broad and quasi-monochromatic spectra and implementation, *J. Atmos. Sol. Terr. Phys.*, *59*, 387–400.

Holton, J. R. (1983), The influence of gravity-wave breaking on the general-circulation of the middle atmosphere, *J. Atmos. Sci.*, *40*, 2497–2507.

Hourdin, F., et al. (2006), The LMDZ4 general circulation model: Climate performance and sensitivity to parametrized physics with emphasis on tropical convection, *Clim. Dyn.*, *27*, 787–813, doi:10.1007/s00382-006-0158-0.

Jourdain, L., S. Bekki, F. Lott, and F. Lefevre (2008), The coupled chemistry climate model LMDz Reprobus: Description of a transient simulation of the period 1980–1999, *Ann. Geophys.*, *26*, 1391–1413.

Kim, Y. H., A. C. Bushell, D. R. Jackson, and H. Y. Chun (2013), Impacts of introducing a convective gravity-wave parameterization upon the QBO in the Met Office Unified Model, *Geophys. Res. Lett.*, *40*, 1873–1877, doi:10.1002/grl.50353.

Lindzen, R. S. (1981), Turbulence and stress owing to gravity wave and tidal breakdown, *J. Geophys. Res.*, *86*, 9707–9714.

Lindzen, R. S., and J. R. Holton (1968), A theory of the quasi-biennial oscillation, *J. Atmos. Sci.*, *25*, 1095–1107.

Lindzen, R. S., and C. Y. Tsay (1975), Wave structure of the tropical stratosphere over the Marshall islands area during 1 April–1 July 1958, *J. Atmos. Sci.*, *32*, 2008–2021.

Lott, F. (1999), Alleviation of stationary biases in a GCM through a mountain drag parametrization scheme and a simple representation of mountain lift forces, *Mon. Wea. Rev.*, *127*, 788–801.

Lott, F. (2003), Large-scale flow response to short gravity waves breaking in a rotating shear flow, *J. Atmos. Sci.*, *60*, 1691–1704.

Lott, F., and M. Miller (1997), A new subgrid scale orographic drag parameterization; its testing in the ECMWF model, *Q. J. R. Meteorolog. Soc.*, *123*, 101–127.

Lott, F., and H. Teitelbaum (1992), Nonlinear dissipative critical level interaction in a stratified shear flow: Instabilities and gravity waves, *Geophys. Astrophys. Fluid Dyn.*, *66*, 133–167.

Lott, F., L. Fairhead, F. Hourdin, and P. Levan (2005), The stratospheric version of LMDz: Dynamical climatologies, Arctic oscillation, and impact on the surface climate, *Clim. Dyn.*, *25*, 851–868, doi:10.1007/s00382-005-0064-x.

Lott, F., L. Guez, and P. Maury (2012), A stochastic parameterization of non-orographic gravity waves, formalism and impact on the equatorial stratosphere, *Geophys. Res. Lett.*, *39*, L06807, doi:10.1029/2012GL051001.

Martin, A., and F. Lott (2007), Synoptic responses to mountain gravity waves encoutering directional critical levels, *J. Atmos. Sci.*, *64*, 828–848, doi:10.1175/JAS3873.1.

McLandress, C., and T. G. Shepherd (2009), Simulated anthropogenic changes in the Brewer-Dobson circulation, including its extension to high latitudes, *J. Clim.*, *22*, 1516–1549, doi:10.1175/2008JCLI2679.1.

McLandress, C., J. F. Scinocca, T. G. Shepherd, M. C. Reader, and G. L. Manney (2013), Dynamical control of the mesosphere by orographic and non-orographic gravity wave drag during the extended northern winters of 2006 and 2009, *J. Atmos. Sci.*, *70*, 2152–2169.

Manzini, E., N. A. McFarlane, and C. McLandress (1997), Impact of the Doppler spread parameterization on the simulation of the middle atmosphere circulation using the MA/ECHAM4 general circulation model, *J. Geophys. Res.*, *102*(D22), 25,751–25,762, doi:10.1029/97JD01096.

Maury, P., F. Lott, L. Guez, and J.-P. Duvel (2013), Tropical variability and stratospheric equatorial waves in the IPSLCM5 model, *Clim. Dyn.*, *40*, 2331–2344, doi:10.1007/s00382-011-1273-0.

Martin, A., and F. Lott (2007), Synoptic responses to mountain gravity waves encoutering directional critical levels, *J. Atmos. Sci.*, *64*, 828–848, doi:10.1175/JAS3873.1.

Naujokat, B. (1986), An update of the observed quasi-biennial oscillation of the stratospheric winds over the tropics, *J. Atmos. Sci.*, *43*, 1873–1877.

Orr, A., P. Bechtold, J. Scinocca, M. Ern, and M. Janiskova (2010), Improved middle atmosphere climate and forecasts in the ECMWF Model through a nonorographic gravity wave drag parameterization, *J. Clim.*, *23*, 5905–5926.

Palmer, T. N., G. J. Shutts, and R. Swinbank (1986), Alleviation of systematic westerly bias in general circulation and numerical weather prediction models through an orographic gravity wave drag parametrization, *Q. J. R. Meteorolog. Soc.*, *112*, 2056–2066.

Palmer, T. N., G. J. Shutts, R. Hagedorn, F. J. Doblas-Reyes, T. Jung, and M. Leutbecher (2005), Representing model uncertainty in weather and climate prediction, *Annu. Rev. Earth Planet. Sci.*, *33*, 163–193, doi:10.1146/annurev.earth.33.092203.122552.

Piani, C., W. A. Norton, and D. A. Stainforth (2004), Equatorial stratospheric response to variations in deterministic and stochastic gravity wave parameterizations, *J. Geophys. Res.*, *109*, D14101, doi:10.1029/2004JD004656.

Rienecker, M. M., et al. (2011), MERRA: NASAs modern-era retrospective analysis for research and applications, *J. Clim.*, *24*, 3624–3648, doi:10.1175/JCLI-D-11-00015.1.

Richter, J. H., F. Sassi, and R. R. Garcia (2010), Toward a physically based gravity wave source parameterization in a general circulation model, *J. Atmos. Sci.*, *67*, 136–156.

Rind, D., R. Suozzo, N. K. Balachadran, A. Lacis, and G. Russel (1988), The Giss global climate-middle atmosphere model. Part I: Model structure and climatology, *J. Atmos. Sci.*, *45*, 329–370.

Scaife, A. A., N. Butchart, C. D. Warner, and R. Swinbanck (2002), Impact of a spectral gravity wave parameterization on the stratosphere in the Met Office unified model, *J. Atmos. Sci.*, *59*, 1473–1489.

Shutts, G. J. (2005), A kinetic energy backscatter algorithm for use in ensemble prediction systems, *Q. J. R. Meteorolog. Soc.*, *131*, 3079–3102.

Scinocca, J. F. (2003), An accurate spectral nonorographic gravity wave drag parameterization for general circulation models, *J. Atmos. Sci.*, *60*, 667–682.

Song, I.-S., and H.-Y. Chun (2005), Momentum flux spectrum of convectively forced internal gravity waves and its application to gravity wave drag parameterization, Part I: Theory, *J. Atmos. Sci.*, *62*, 107–124.

Song, I.-S., H.-Y. Chun, R. R. Garcia, and B. A. Boville (2007), Momentum flux spectrum of convectively forced internal gravity waves and its application to gravity wave drag parameterization. Part II: Impacts in a GCM (WACCM), *J. Atmos. Sci.*, *64*, 2286–2308.

Souprayen, C., J. Vanneste, A. Hertzog, and A. Hauchecorne (2001), Atmospheric gravity-wave spectra: A stochastic approach, *J. Geophys. Res.*, *106*, 24,071-24,086.

Takahashi, M., and B. A. Boville (1992), A three-dimensional simulation of the equatorial quasi-biennial oscillation, *J. Atmos. Sci.*, *49*, 1020–1035.

Takahashi, M. (1999), Simulation of the stratospheric quasi-biennial oscillation in a general circulation model, *Geophys. Res. Lett.*, 1307–1310.

Warner, C. D., and M. E. McIntyre (1996), On the propagation and dissipation of gravity wave spectra through a realistic middle atmosphere, *J. Atmos. Sci.*, *53*, 3213–3235.